Electronic Supplementary Material (ESI) for Energy & Environmental Science.

Supporting Information

Synthesis of Porous and Metallic CoB Nanosheets towards Highly Efficient Electrocatalyst for Rechargeable Na-O_2 Batteries

Experiment

1. Chemicals and materials

Commercial Carbon nanotube (CNT) was purchased from Tianjin; Poyvinylidene fluoride (PVDF, 99.9%, DuPont Company); N-methyl-2-pyrrolidinone (NMP, Aladdin Reagent, AR); Tretraethylene glycol dimethyl ether (TEGDME, Aladdin Reagent, AR); Sodium trifluoromethanesulfonate ($NaCF_3SO_3$, Aladdin Reagent, 98%); Carbon paper (CP, TGP-H-060, Torray); Glassy carbon rotating electrode (GC, 5 mm in diameter) was purchased from Tianjin AidaHengsheng Tech. Co., China; Anhydrous cobalt chloride ($CoCl_2$, Aladdin Reagent, AR); Sodium borohydride ($NaBH_4$, HEOWNS Reagent, Tianjin, China); Anhydrous lithium chloride (LiCl, Aladdin Reagent, AR); Potassium chloride (KCl, Aladdin Reagent, AR).

2. Preparation of CoB catalyst

The electrocatalyst CoB-900 was synthesized by heat treatment the mixture of $CoCl_2$, $NaBH_4$ and LiCl: KCl (45:55 wt%). In a typical procedure, 1 mmol of anhydrous $CoCl_2$ and 8 mmol of anhydrous $NaBH_4$ are mixed with 2.5 g of eutectic salt LiCl: KCl and grounded in glove box. Then the obtained mixture was molten in a porcelain crucible and heated for 4 hours at 900 °C with flowing Ar. The heating rate was fixed at 5 °C/min. As for preparing CoB-800 or CoB-1000, the ratio of precursors still retains, and it just adjusts heat treatment temperature to 800 or 1000 °C. For perparing CoB (1:4) or CoB (1:12), the ratio of $CoCl_2$ to $NaBH_4$ should be adjusted to 1:4 or 1:12, and the heat treatment temperature keeps at 900 °C.

3. Calculation Method

The first principle calculations based on density functional theory (DFT) were carried out by using the Vienna ab initio simulation package (VASP),[1] with exchange-correlation functional described by

Perdew Burke-Ernzerhof generalized gradient approximation (PBE-GGA) and interaction between core electrons and valence electrons by the frozen-core projector-augmented wave (PAW) method. An energy cut-off of 500 eV was used for plane wave basis expansion. We employed a 0.1 eV smearing of the Fermi-level and (9×9×9) K-points for bulk calculations and (3×3×1) for surfaces. All the atoms were relaxed with a force tolerance of 0.01 eVÅ^{-1} and an energy convergence of 1×10^{-6} eV. The spin polarization was considered for the existence of Co.

Models: According to the previous studies,[2] we chose the graphene (G) to substitute the CNT in this study. A 5×5 supercell was built for the G with 50 atoms. The Na_2O_2 (001) surface with four layers and a 3×2 supercell of CoB (010) surface with three layers were constructed from their crystal structures, respectively. A vacuum region of around 15 Å was set along the z direction for the surfaces to avoid the interaction between periodic images.

Mechanism analysis: Thermodynamic potentials for charging were deduced by calculating free energies of all intermediates. We assumed $Na^+ + e^-$ are in electrochemical equilibrium at U= 0 V with a bulk Na metal. We assumed the electrochemical potential of an electron shift by -eU when the electrode potential U sets in according to Nernst equation (U= -ΔG/ne), where ΔG is the change of Gibbs free energy, n is the number of electrons involved with the electrochemical reaction, and the e is elementary charge.

The reaction free energy of intermediate steps was calculated by

$$\Delta G = E - E_0 + \Delta N_{Na}(\mu_{Na} - eU) + \Delta N_{O_2}\mu_{O_2}$$

where E is the total energy of the considered slab model, E_0 is the total energy of the initial slab model, ΔN_{Na} and ΔN_{O_2} are the numbers of sodium atoms and oxygen molecules removed for each step, and μ_{Na} and μ_{O_2} are the chemical potentials of sodium bulk and oxygen, respectively. The eU term was added to account for the electronic energy under applied potential U.

4. Electrochemical performance measurement

The cathodes were prepared by coating homogenous ink composed of the mixture of 30 wt% CoB catalyst, 60 wt% CNT, and 10 wt% polyvinylidene fluoride (PVDF) or 90 wt% CNT and 10 wt% PVDF onto the carbon paper current collector. Then the cathodes were dried in a vacuum oven at 80 °C for 24 h. The total mass (CNT or CoB/CNT cathode) on the carbon paper current collector is about 0.50 ± 0.10 mg. For electrolyte, TEGDME solvent was soaked in activated molecular sieves (4 Å type) for 15 days until the water content below 10 ppm. $NaCF_3SO_3$ was heated at 80 °C in vacuum oven for 24 hours. The electrolyte contains 0.5 M $NaCF_3SO_3$ in TEGDME solvent (H_2O < 10 ppm). All the cells were assembled in a glove box under argon atmosphere using modified 2025-type coin cell whose top covers with nine holes of 2 mm in diameter that permit the diffusion of the oxygen (**Fig. S22**). A sodium metal foil anode (Φ=14 mm), a glass fiber separator (Φ = 16 mm), the prepared CNT or CoB/CNT cathodes (Φ=12 mm) and 80 μL electrolyte were combined in sequence. The assembled batteries were purified by the straight two-way piston conducted alternatively by vacuuming and ventilating three times with high-purity O_2. After that, the purified batteries was pumped into 250 mL O_2 and then were settled for 3 hours before electrochemical measurement. The Na-O_2 cells were subjected to linear sweep voltammetry (LSV) and electrochemical impedance spectroscopy (EIS) test using an AC impedance analyzer on a Biologic VMP3 electrochemical workstation at room temperature. LSV test was carried out at a scan rate of 5 mV s^{-1} in the range of 2.0–4.0 V versus Na^+/Na. The galvanostatic tests were conducted at a current density of 100 mA g^{-1} with a fixed capacity of 2000 mAh g^{-1} in the range of 1.6-4.0 V (vs. Na/Na^+) using a LAND CT2001A multi-channel batteries testing system. All the electrochemical tests were carried out under 1 atm pure oxygen (99.999%) chamber. In this work, both the applied current density (mA g^{-1}) and calculated specific capacity (mAh g^{-1}) are based on the total mass of the catalyst and CNT excluding current colloctor CP.

Electrochemical surface area (ECSA) measurements[3]: ESCA is calculated by the equation: ECSA = $R_f \cdot S$, wherein R_f is the roughness factor, and S is the geometric area of the cathode (in our work, S = 1.13 cm^2). R_f is the ratio of double-layer capacitance (C_{dl}) for sample relative to that of geometric planar (here assuming that the average double-layer capacitance of a flat electrode is 60 μF cm^{-2}). The C_{dl} for sample was determined by using a simple CV method. Na metal was used as the counter electrode and reference electrode. 0.5 M $NaCF_3SO_3$/TEGDME was used as the electrolyte. CV curves at different scan rates (1 mV s^{-1}, 2 mV s^{-1}, 4 mV s^{-1}, 8 mV s^{-1} and 10 mV s^{-1}) were obtained in the potential region (0.9~1.1 V) where non-faradaic processes occurred. The slope of the current density versus scan rates yielded the double-layer capacitance value as shown in Fig. S23 and Table S1.

5. Instrumentation

Powder X-ray diffraction (XRD) measurements were performed on Bruker D8 Focus Powder X-ray diffractometer using Cu Kα radiation (40 kV, 40 mA). Scanning electron microscopy (SEM) was conducted on a field emission Hitachi S-4800 instrument, operating at an accelerating voltage of 10 kV. Transmission electron microscope (TEM) was performed using a FEI Tecnai G2 S-Twin instrument with a field emission gun operating at 200 kV. 1Hydrogen-nuclear magnetic resonance spectra (1H-NMR) were performed on a Bruker Avance II 400 spectrometer. For in-situ differential electrochemical mass spectrometry measurement, a Na-O_2 battery (EL-CELL GmbH) was linked to a commercial magnetic sector mass spectrometer (Hiden Analytical) by a specially designed gas-purging system. High-purity Ar was used as the carrier gas and the flow rate of purge gas was set at 1 mL min^{-1}. Nitrogen adsorption measurements were performed on a Micromeritics ASAP 2020 adsorption analyzer. Specific surface areas were calculated by the Brunaure-Emmert-Teller (BET) method. Pore volumes and sizes were estimated from pore size distribution curves from the adsorption isotherms using the Barrett-Joyner-Halenda (BJH) method. XPS spectra were obtained with ESCALAB MK II X-ray photoelectron

spectrometer using an Al Kα source. The absorbance datum of spectrophotometer was measured on Beijing Purkinje General, TU-1900. The electrical conductivity was record using a Keithley 2400 sourcemeter characterization system by a four-point probe configure. Raman scattering spectra were recorded using a Nicolet 380 and a HORIBA Scientific LabRAM HR Raman spectrometer system equipped with a 533 nm laser.

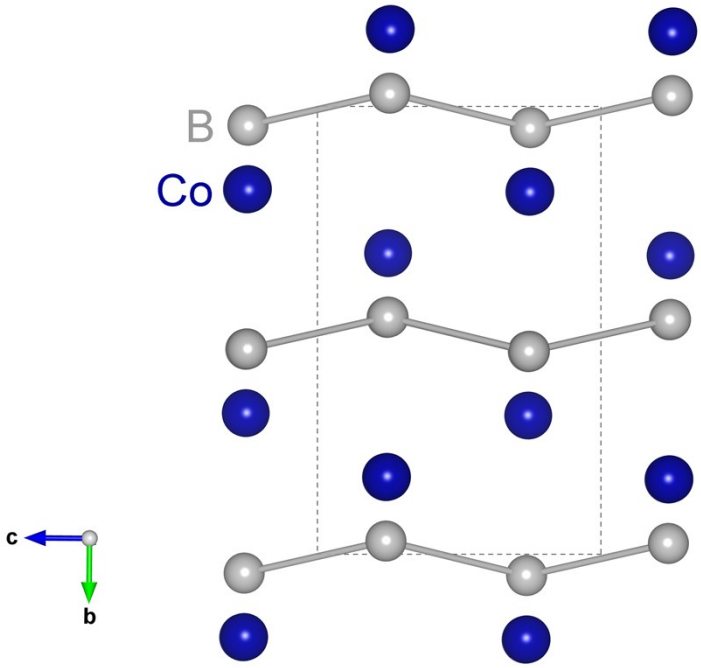

Fig. S1 Schematic crystal structure of CoB.

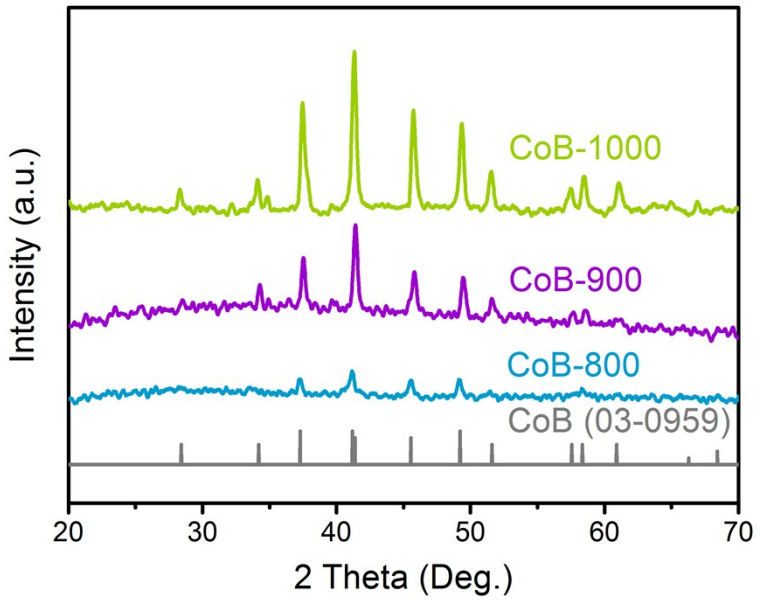

Fig. S2 X-ray diffraction patterns of CoB formed at different heat temperatures with the cobalt chloride and sodium borohydride (1:8) precursors.

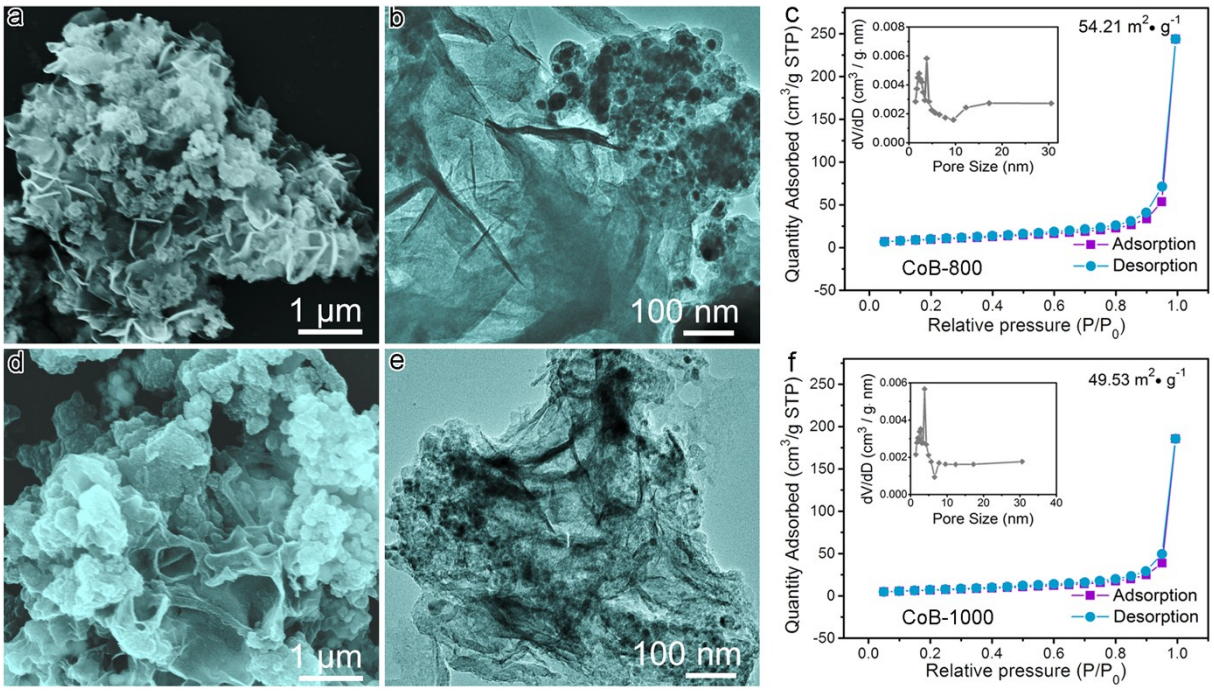

Fig. S3 SEM, TEM images and nitrogen adsorption–desorption isotherms (inset: pore size distribution) of CoB after heat treatment at a, b, c) 800 ºC, and d,e,f)1000 ºC.

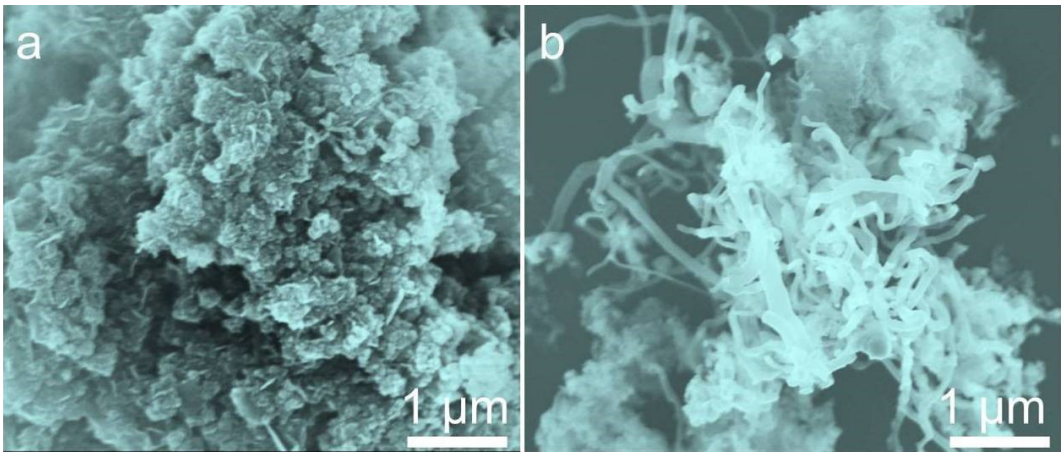

Fig. S4 SEM images of CoB after heat treatment at 900 ºC with different molar ratio of anhydrous $CoCl_2$ to $NaBH_4$ with a) 1:4, and b) 1:12.

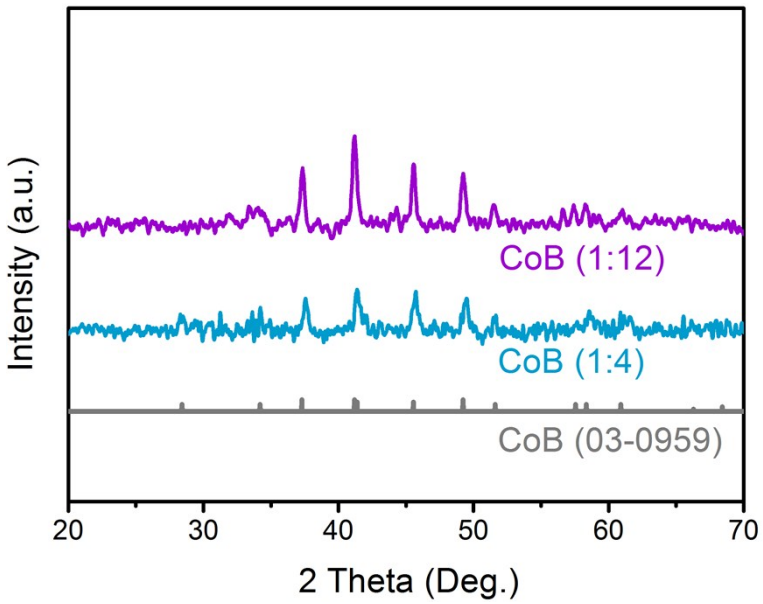

Fig. S5 XRD patterns of CoB after heat treatment (900 ºC) with different molar ratios of anhydrous $CoCl_2$ to $NaBH_4$.

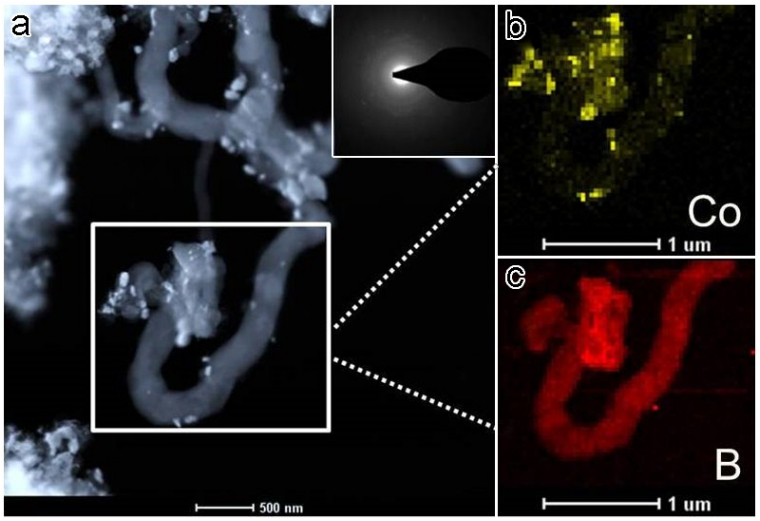

Fig. S6 a) TEM images (insert: the according selected area electron diffraction), and the corresponding element mapping images of Co b), and B c) for CoB (1:12).

As shown in S6, with the increase of B sources (1:12), amorphous B tubes appear according to the selected area electron diffraction and element mapping images results. Therefore, the ratio of the raw materials have decisive role for the preparation of CoB porous sheets.

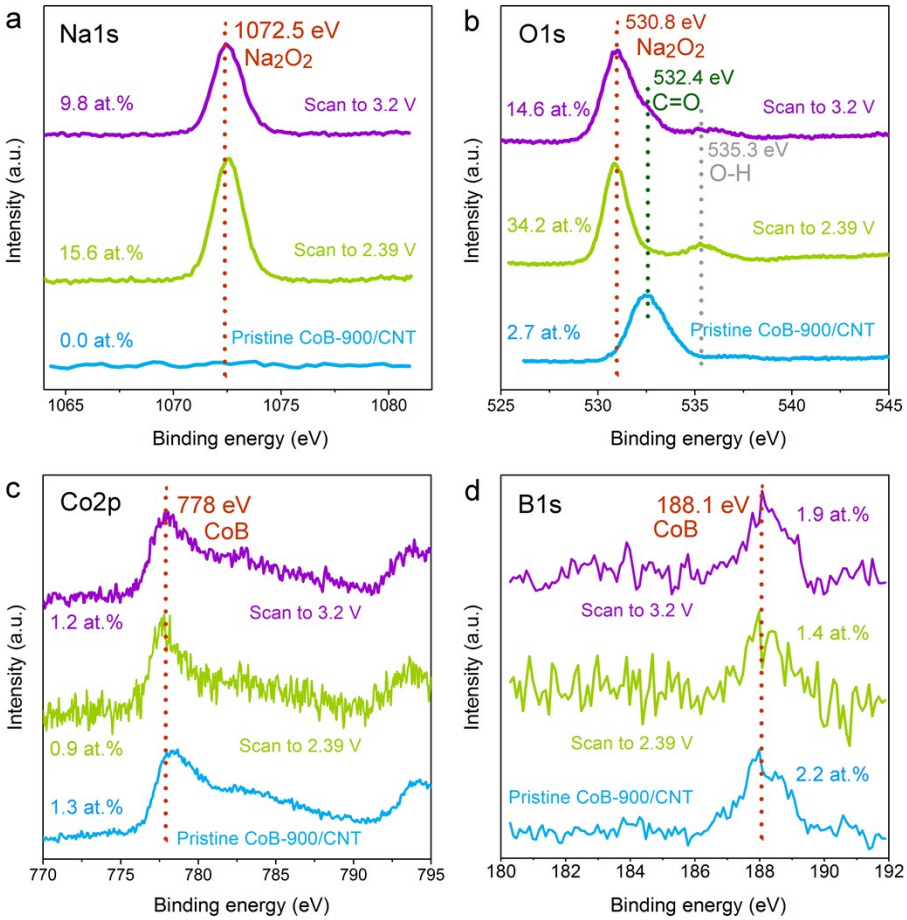

Fig. S7 a) Na1s, b) O1s, c) Co2p, and d) B1s spectra for CoB-900/CNT cathode during LSV measurement.

During LSV measurement, both O and Na content increase compared with that of the pristine CoB-900/CNT, demonstrating ORR products formation; when scanning to 3.2 V, they show some decrease, indicating OER occurrence. O1s spectra at 530.8 eV show Na_2O_2 formation when scanning to 2.39 V, consistent with the ever report.[4] The peaks at 532.4 and 535.3 eV for O1s specra are attributed to C=O and H_2O, which possibly results from incompletely carbonized CNT and crystal water in ORR products, respectively.[5] There is no significant content variation and new peak appearance for Co2p and B1s spectra, displaying the stability of CoB during LSV test.

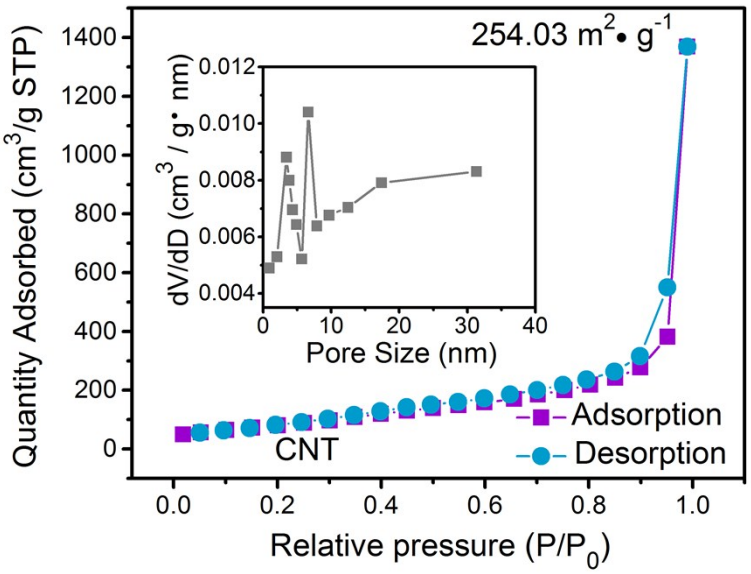

Fig. S8 Nitrogen adsorption–desorption isotherms (insert: pore size distribution) of commercial CNT.

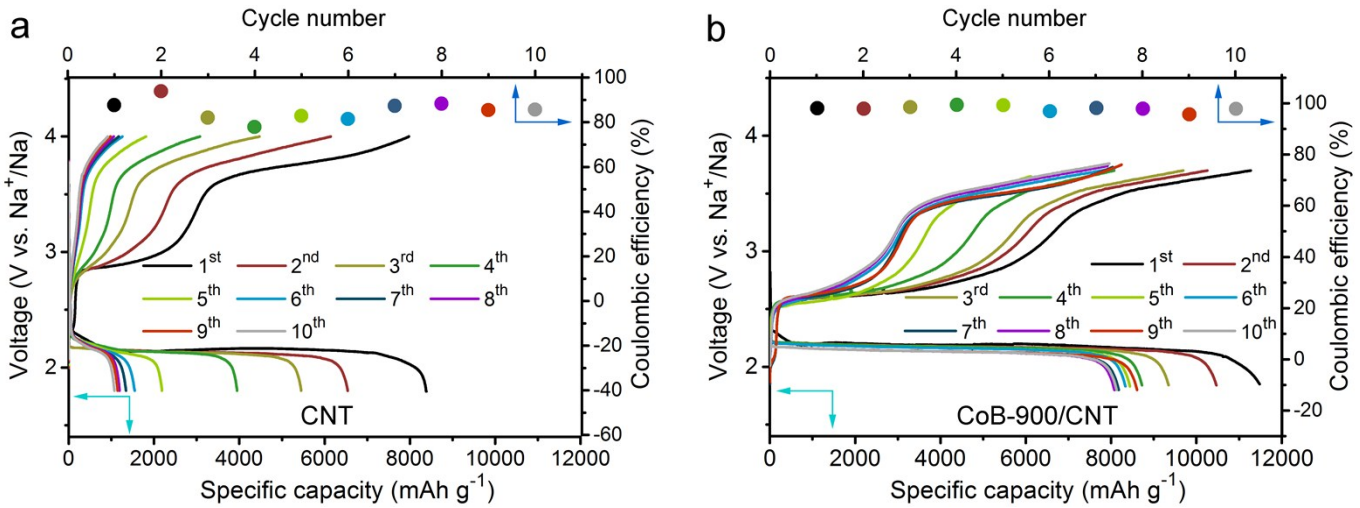

Fig. S9 Free discharge-charge curves of Na-O_2 batteries with a) CNT, and b) CoB-900/CNT cathode as well as the corresponding Columbic efficiency for every cycle.

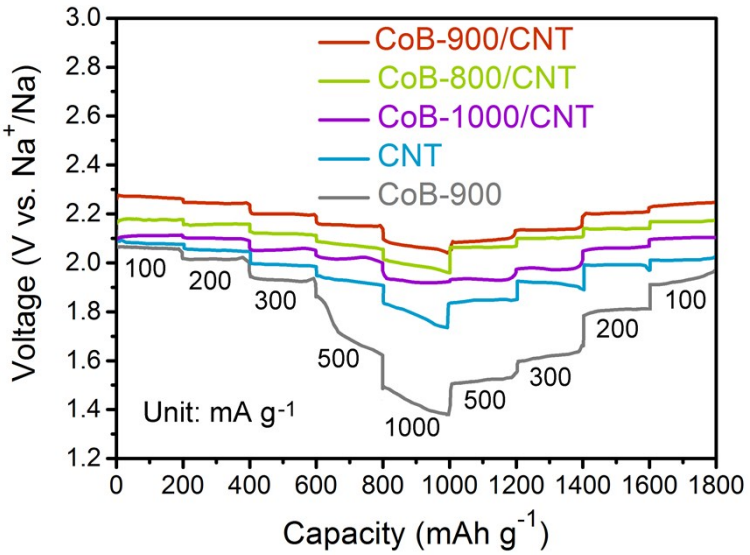

Fig. S10 Rate performance of Na-O_2 batteries with pure CNT, CoB, CoB-800/CNT, CoB-900/CNT, and CoB-1000/CNT composited cathodes under different current densities.

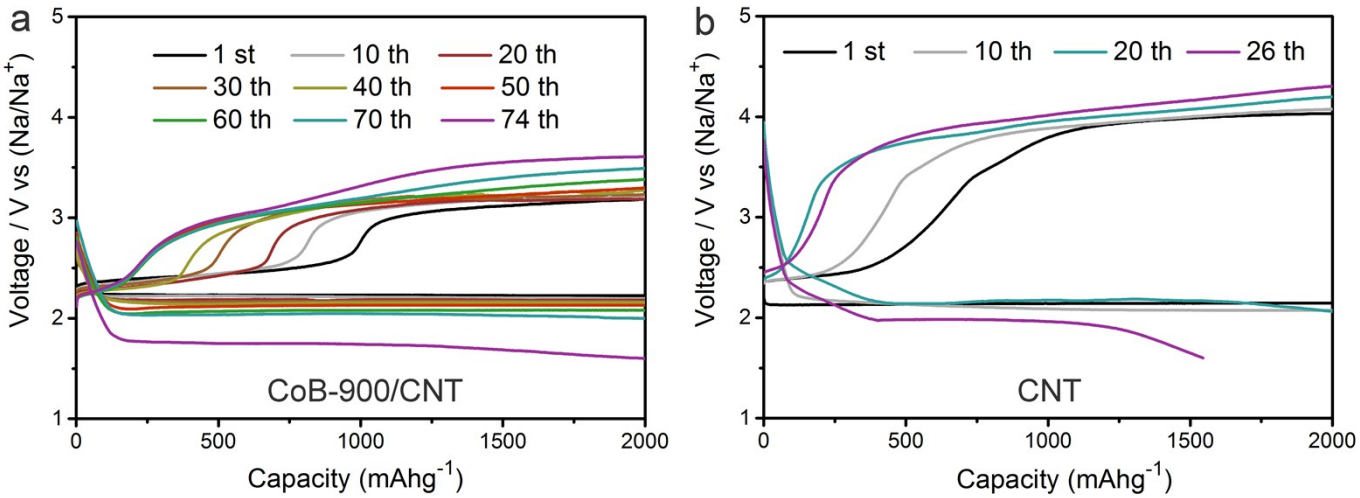

Fig. S11 The specific discharge-charge curves of the Na–O_2 batteries from Figure 4d with the a) composited CoB-900/CNT, and b) pure CNT cathode at a limited current density of 100 $mA \cdot g^{-1}$.

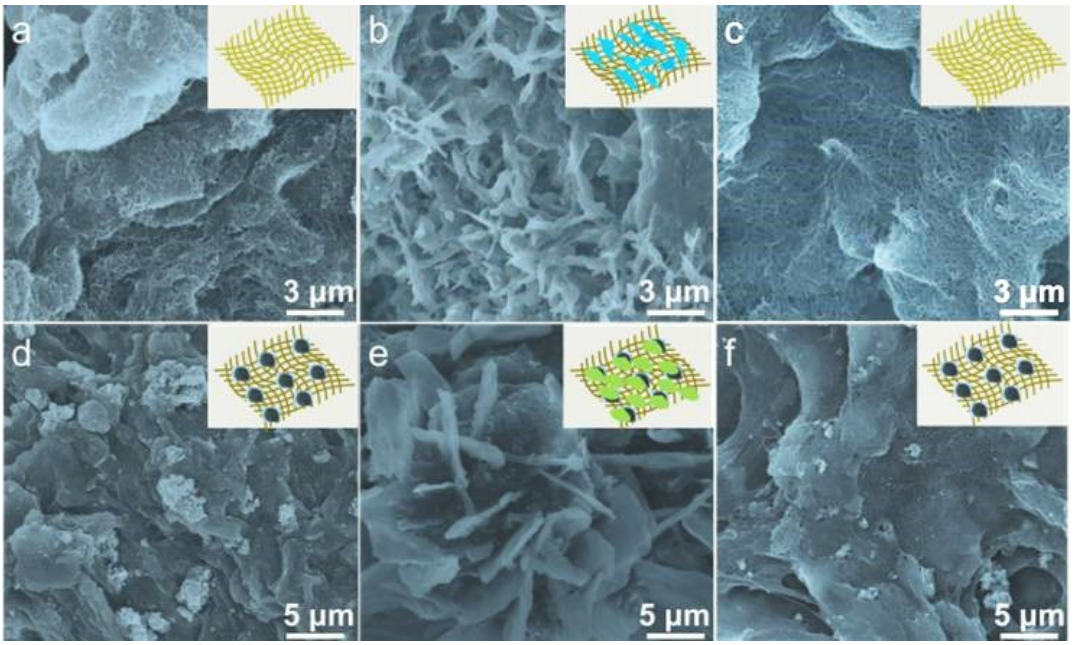

Fig. S12 SEM images of CNT cathode at the a) pristine, b) first discharged, and c) first charged; SEM images of CoB-900/CNT cathode at the d) pristine, e) first discharged, and f) first charged.

If all the discharge products are film, and they fully cover the surface areas of the cathode, the thickness of the NaO_2 and Na_2O_2 layer on the cathode can be calculated as follow: the total mass of cathode is 0.5 mg, wherein it contains 33 % CoB (electrochemical surface ares: 50.3 $m^2\ g^{-1}$) and 67 % CNT (electrochemical surface ares: 114 $m^2\ g^{-1}$). Therefore, the whole surface areas of the cathode is: $0.5*10^{-3}*0.33*50.3\ m^2\ g^{-1} + 0.5*10^{-3}*0.67*114\ m^2\ g^{-1}=4.65*10^{-2}\ m^2=465\ cm^2$; the density of Na_2O_2 and NaO_2 are 2.8 g cm^{-3} and 2.2 g cm^{-3}, respectively; if all the discharge products are Na_2O_2, the thickness of discharge products on cathode would be: $(11482*0.5*10^{-3}*3.6*78)/(96485*2.8*465)=1.28*10^{-5}$cm=128 nm; if all the discharge products are NaO_2, the thickness of discharge products on cathode would be: $(11482*0.5*10^{-3}*3.6*55)/(96485*2.2*465)=1.15*10^{-5}$ cm=115 nm. Actually, the discharge products are not film-like but sheet-like with only one side contacting with cathode, so the real thickness of discharge products is much less than 128 nm. The cathode can efficiently catalyze products to decompose even at such high capacities.

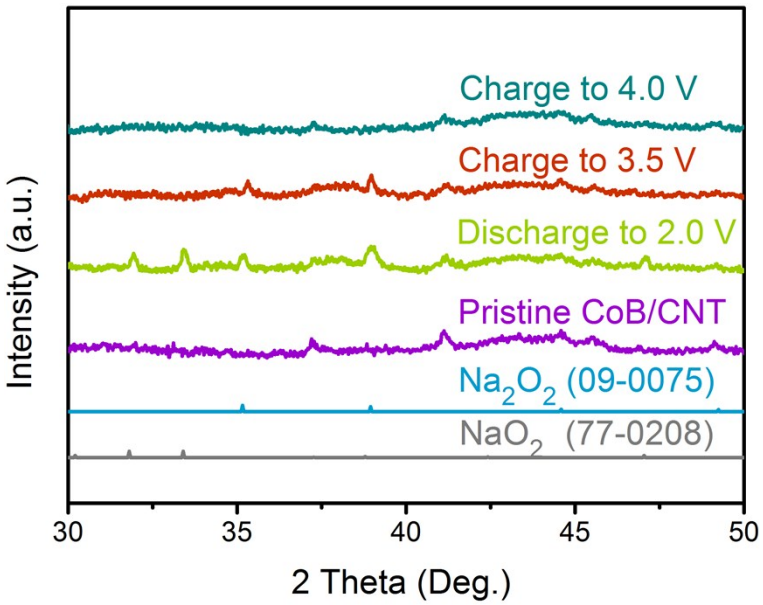

Fig. S13 XRD patterns of CoB-900/CNT cathode at different electrochemical conditions.

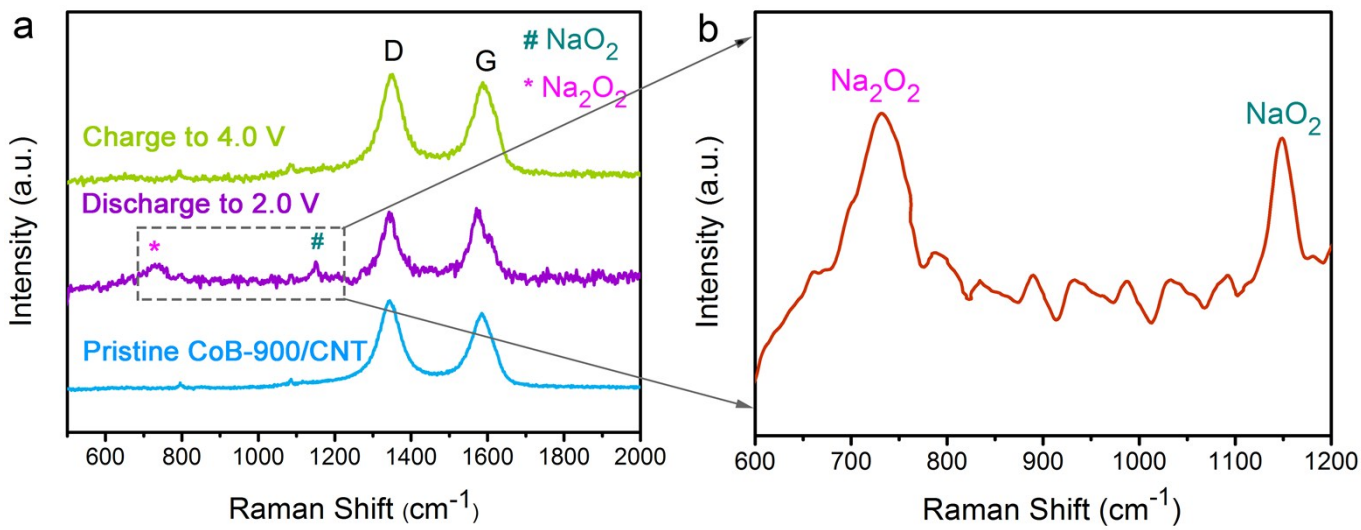

Fig. S14 Raman spectra of a) CoB-900/CNT cathode at different electrochemical conditions, b) the marked area in (a) after enlarging.

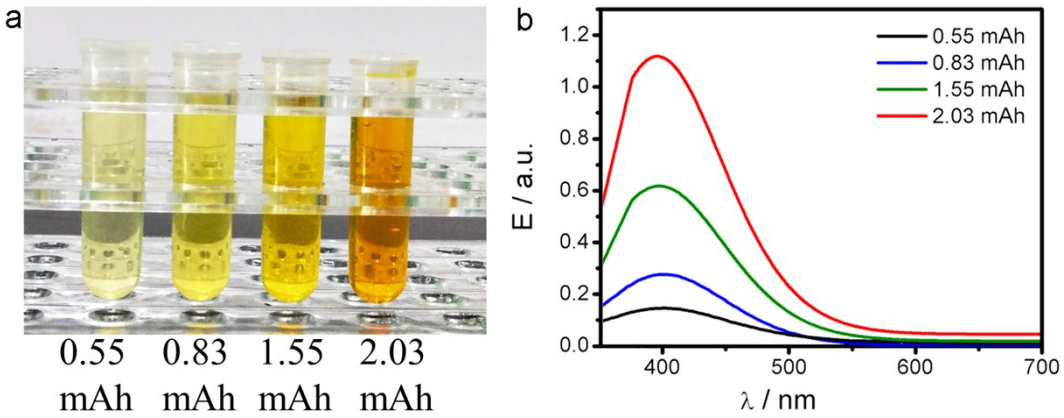

Fig. S15 a) Photograph of aqueous $TiOSO_4$ solution after reacting with the discharged CoB-900/CNT cathodes under different capacity. The yellow color results from the formation of $[Ti(O_2^{2-})]^{2+}$ complex due to the presence of O_2^{2-} derived from the hydrolysis of NaO_2 and Na_2O_2; and b) The corresponding extinction of the $TiOSO_4$ solutions.

To determine the discharge products, we employed an UV/Vis spectroscopic analysis. All the alkali-metal oxides can react with the H_2O to form H_2O_2 which can turn the colourless $TiOSO_4$ solution to yellow due to the formation of a $[Ti(O_2^{2-})]^{2+}$ complex, with a light absorption maximum at around 405 nm.[6]

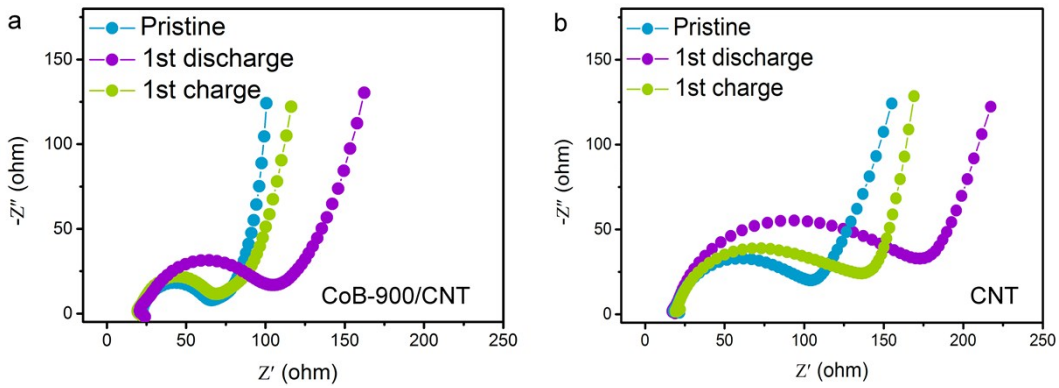

Fig. S16 EIS for Na-O_2 batteries at different electrochemical states with the a) composited CoB-900/CNT, and b) pure CNT cathodes.

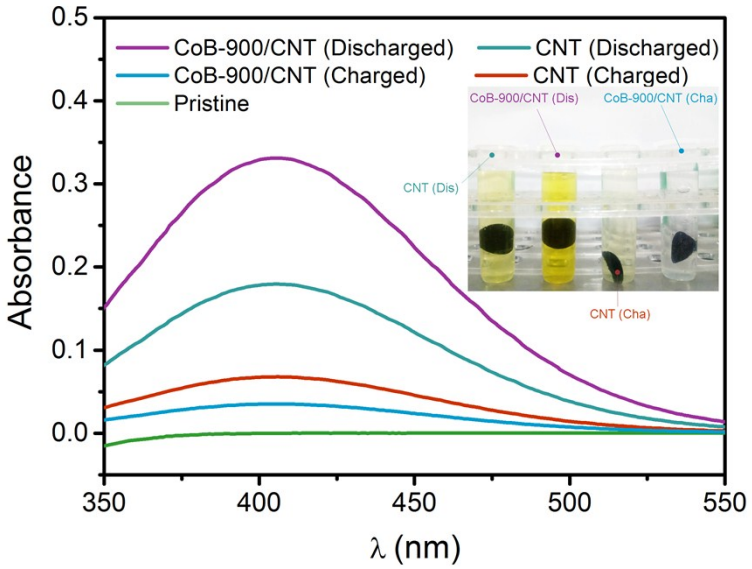

Fig. S17 The absorbance curves of the $TiOSO_4$ solutions with the CoB-900/CNT and CNT cathodes undergoing different electrochemical process (inset: the corresponding photograph of $TiOSO_4$ solution).

UV/Vis spectroscopic analysis is based on the principle wherein alkali-metal peroxides and super oxides react with water to form hydrogen peroxide as shown in the following reactions:

$$Na_2O_2 + 2H_2O = 2NaOH + H_2O_2$$

$$2NaO_2 + 2H_2O = 2NaOH + H_2O_2 + O_2$$

In the presence of H_2O_2, the colorless $TiOSO_4$ solution solutions turn yellow due to the formation of a $[Ti(O_2^{2-})]^{2+}$ complex, with a light absorption maximum at around 405 nm. According to the above reactions, we can find that every two molars electron transfer can generates 1 molar H_2O_2. Therefore, no matter forming 1 molar Na_2O_2 with two molar electron transfer or 2 molar NaO_2 with two molar electron transfer, the generated H_2O_2 is same, i.e. the same number of electron transfer calculated basing on H_2O_2.

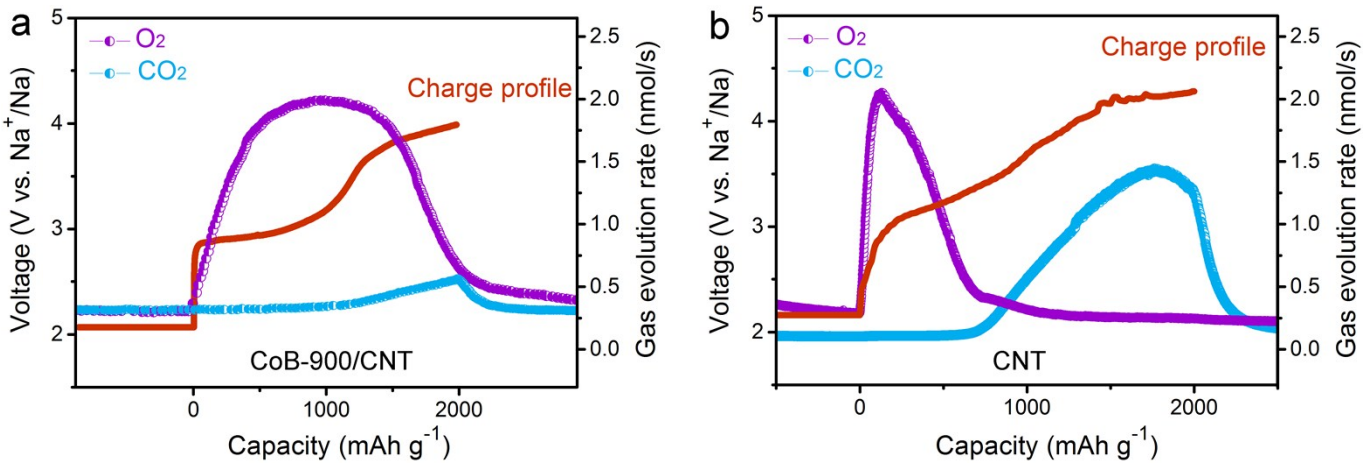

Fig. S18 Gas evolution from the Na-O_2 cell with a) CoB-900/CNT, and b) CNT cathode at a current density of 400 mA g^{-1}.

According to the gas evolution curves, we can observe large amounts of O_2 evolution, far higher than CO_2, indicating greatly suppressed side reaction for CoB-900/CNT cathode. In sharp contrast, with CNT cathode, CO_2 evolution is much more than O_2 evolution, demonstrating the poor catalytic activity of CNT cathode towards ORR and/or the intrinsic poor capability of decomposing sodium oxides.

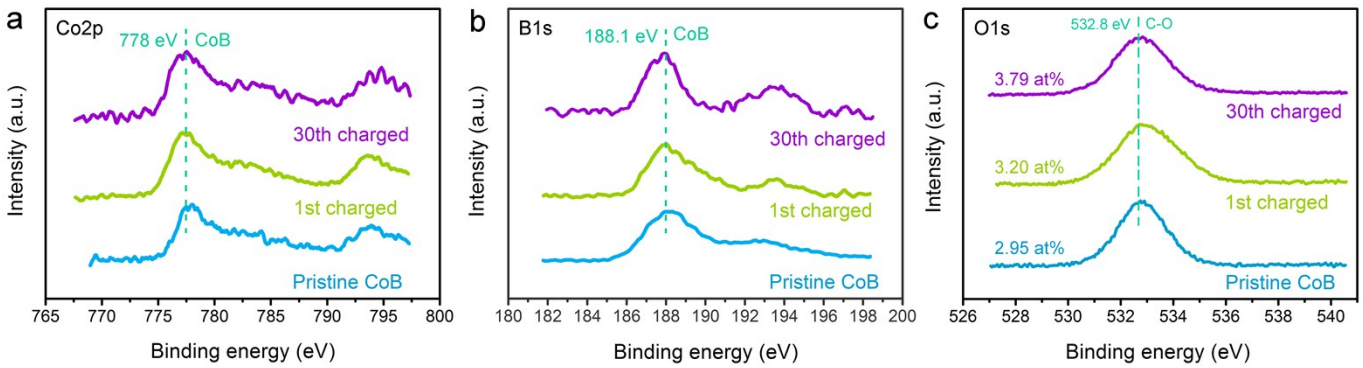

Fig. S19 Co2p a), B1s b), and O1s c) spectra for the cycled CoB-900.

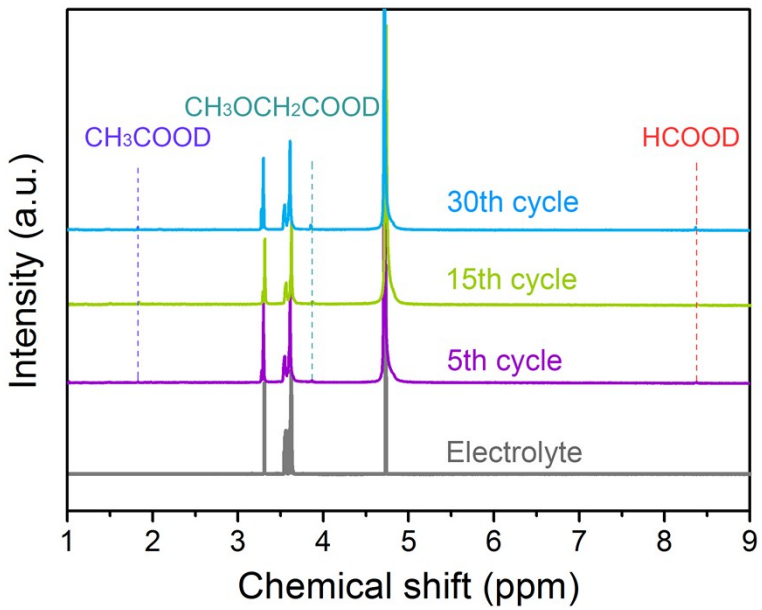

Fig. S20 1H-NMR spectra of CoB-900/CNT cathode at different electrochemical conditions.

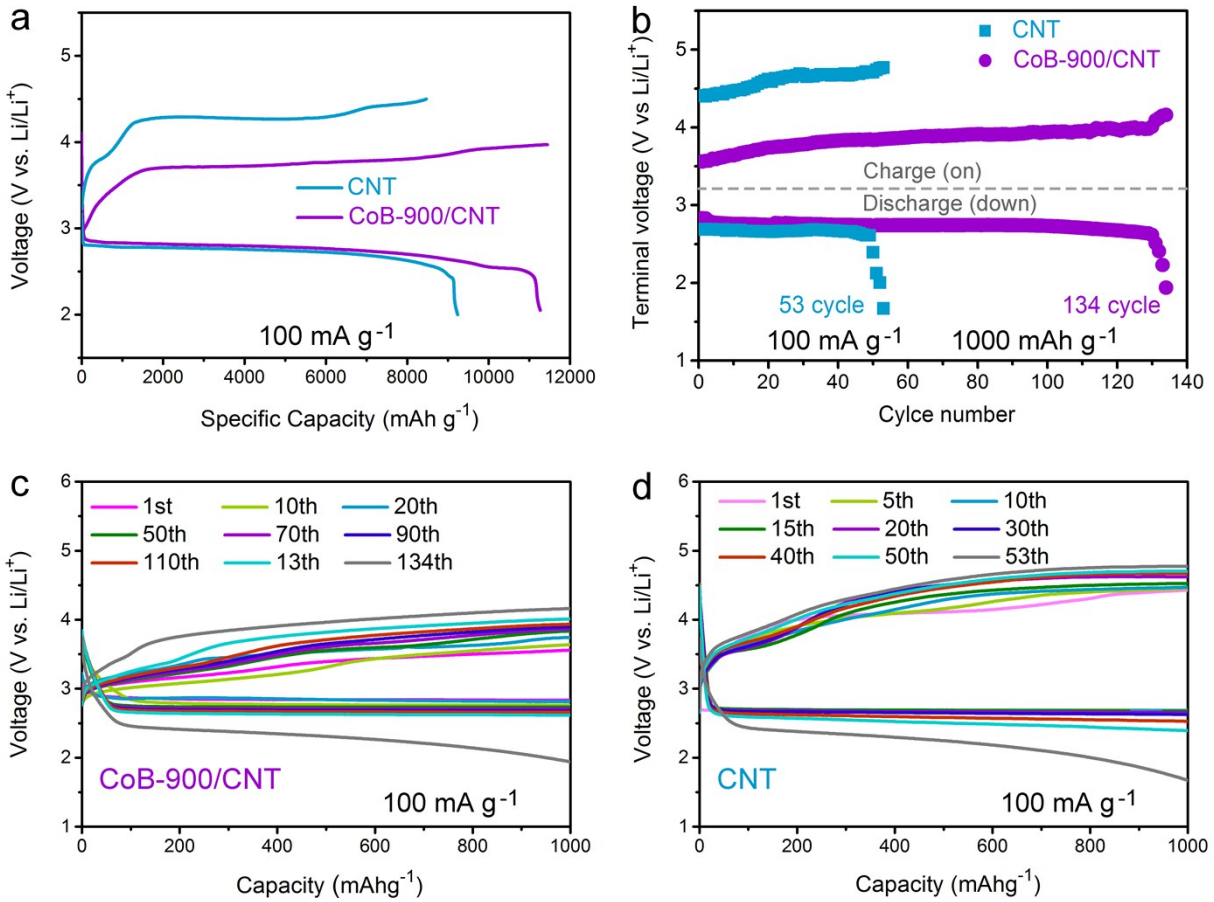

Fig. S21 Free discharge-charge curves a), voltage of the terminal discharge and charge vs. cycle number b), and the specific discharge-charge cycle curves c, d) of the Li–O_2 batteries with the composited CoB-900/CNT and pure CNT cathode, respectively at a limited current density of 100 mA·g^{-1}.

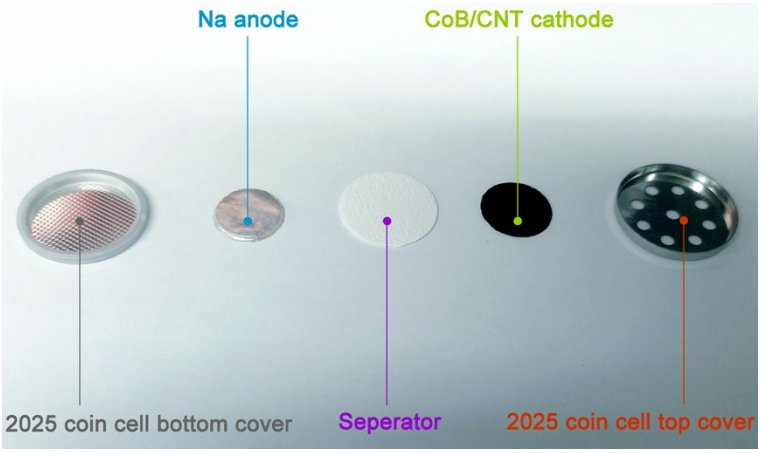

Fig. S22 Photograph of modified 2025-type coin cell used in Na-O_2 batteries.

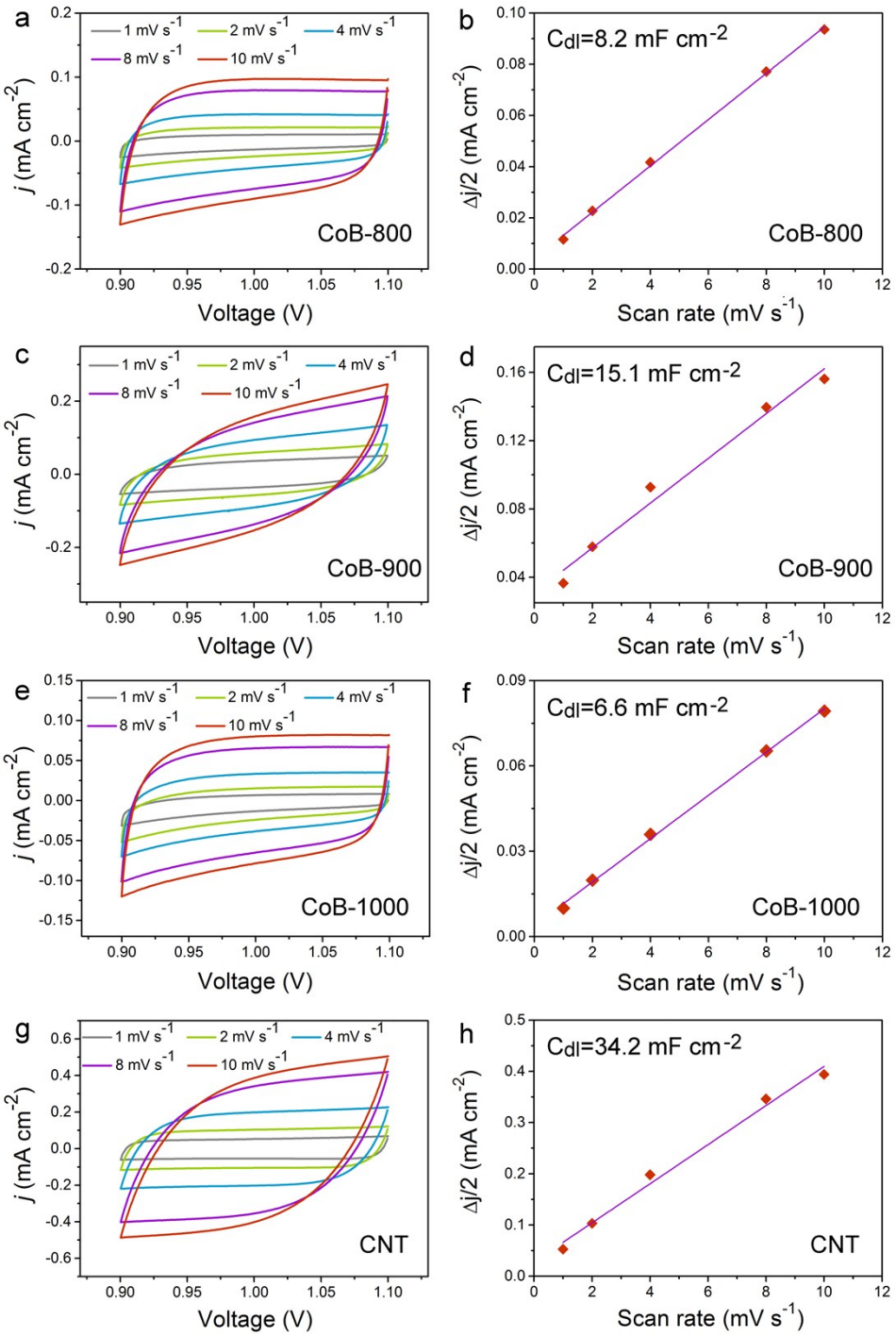

Fig. S23 Cyclic voltammograms in the region of 0.9~1.1 V vs. Na^+/Na at various scan rates and the corresponding linear fitting of the capacitive currents vs. scan rates to estimate the C_{dl} for a, b) CoB-800; c, d) CoB-900; e, f) CoB-1000, and g, h) CNT; and the calculated C_{dl} values are shown in the insets.

Table S1. The ECSA and BET surface areas for CoB-800, CoB-900, CoB-1000, and CNT, respectively.

Sample	ECSA (m^2 g^{-1})	BET surface area (m^2 g^{-1})
CoB-800	30.9	54.2
CoB-900	56.9	128.1
CoB-1000	24.9	49.5
CNT	128.8	254.0

Table S2. The electronic conductivity of the pure CNT, CoB-900, composited CoB-1000/CNT, CoB-900/CNT, and CoB-800/CNT cathode, respectively.

Cathode	CNT	CoB-900	CoB-900/CNT	CoB-800/CNT	CoB-1000/CNT
Electronic conductivity (S cm^{-1})	12.8	0.1	8.5	2.2	1.4

Table S3. Summary of reported electrochemical performance of Na-air/O_2 cells with carbon-based cathodes.

Cathode	Loading (mg)	Discharge current density (mA g^{-1})	Discharge capacity (mAh g^{-1})	Cycle life	Limited Capacity for Cycling (mAh g^{-1})	Reference
CoB-900/CNT	0.50 ± 0.10	100	**11482**	74	**2000**	**This work**
CNT@Co3O4	0.25 ± 0.10	150	**720**	15	**300**	[7]
a-MnO2 nanowires @ C	No mention	0.2	**2056**	55	**1100**	[8]
$CaMnO_3$/C	No mention	200	**9560**	80	**1000**	[9]

Table S4. The absolute capacity, specific mass capacity (CoB+CNT or CoB+CNT+CP) of Na-O_2 batterie with the CP current collector, pure CNT, CoB-900, composited CoB-800/CNT, CoB-900/CNT, CoB-1000/CNT cathodes, respectively.

Cathode	Mass (mg)	Absolute capacity (C) /mAh	Surface areas ratio ($S_{CoB-900}/S_{CoB}$)	Specific mass capacity 1 (C1) /mAh $g_{CoB+CNT+CP}^{-1}$	Specific mass capacity 2 (C2) /mAh $g_{CoB+CNT}^{-1}$	The ratio of $(C1_{CoB-900/CNT}-C1_{CNT})/(C1_{CoB/CNT}-C1_{CNT})$
CP current collector	5	1.37	-	249	2740	-
CoB-900	0.5	2.14	-	388	4274	-
pure CNT	0.5	4.21	-	766	8424	-
CoB-800/CNT	0.5	4.62	2.37	839	9230	3.79
CoB-900/CNT	0.5	5.74	1	1044	11482	1
CoB-1000/CNT	0.5	4.51	2.56	820	9026	5.08

The surface areas ratio in Table S4 shows that the surface areas of CoB-900 is several times of its counterparts, while the ratio of $(C_{CoB-900/CNT}-C_{CNT})/(C_{CoB/CNT}-C_{CNT})$ is much higher than the according surface areas ratio. This demonstrates the superiorty of the composited CoB-900/CNT in catalysis. Without CNT conductive agent, the capacity of CoB-900/CNT is only 1534 mAh g^{-1}, while the capacity doubles after adding CNT conductive agent, indicating synergistic effect of CoB-900 and CNT.

Table S5. Height change (∆h) of the mass center of adsorbed Na_2O_2 for decomposing reaction in CoB/Na_2O_2 and CNT/Na_2O_2 interfaces and the corresponding initial distance (d) from Na_2O_2 to catalyst surfaces.

Systems	**d / Å**	**∆h / Å**
CoB(001)/Na_2O_2(001)	2.60	-0.2
CNT/Na_2O_2(001)	3.16	0.1

References:

[1] G. Kresse and J. Furthmüller, *Comput. Mater. Sci.* **1996,** *6,* 15.

[2] a) L. Shi, A. Xu, T. Zhao, *J. Phys. Chem. C* **2016,** *120,* 6356; b) Q. Sun, J. Liu, X. Li, B. Wang, H. Yadegari, A. Lushington, M. N. Banis, Y. Zhao, W. Xiao, N. Chen, J. Wang, T. K. Sham, X. Sun, *Adv. Func. Mater.* **2017,** *27,* 1606662; c)L. Zhong, R. R. Mitchell, Y. Liu, B. M. Gallant, C. V. Thompson, J. Y. Huang, S. X. Mao, Y. Shao-Horn, *Nano lett.* **2013,** *13,* 2209.

[3] a) S. Gao, Y. Lin, X. Jiao, Y. Sun, Q. Luo, W. Zhang, D. Li, J. Yang, Y. Xie, *Nature* **2016,** *529,* 6; b) J. Kibsgaard, Z. Chen, B. N. Reinecke, T. F. Jaramillo, *Nat. Mater.* **2012,** *11,* 963; c) Z. L. Wang, X. F. Hao, Z. Jiang, X. P. Sun, D. Xu, J. Wang, H. X. Zhong, F. L. Meng, X.-B. Zhang, *J. Am. Chem. Soc.* **2015,** *137,* 15070.

[4] H. Yadegari, Y. Li, M. N. Banis, X. Li, B. Wang, Q. Sun, R. Li, T.-K. Sham, X. Cui, X. Sun, *Energy Environ. Sci.* **2014**, *7*, 3747.

[5] H. Yadegari, C. J. Franko, M. N. Banis, Q. Sun, R. Li, G. R. Goward, X. Sun, *J. Phys. Chem. Lett.* **2017,** *8*, 4794.

[6] P. Hartmann, C. L. Bender, J. Sann, A. K. Dürr, M. Jansen; J. Janek, P. Adelhelm; *Phys. Chem. Chem. Phys.* **2013,** *15,* 11661.

[7] Q. Sun, J. Liu, X. Li, B. Wang, H. Yadegari, A. Lushington, M. N. Banis, Y. Zhao, W. Xiao, N. Chen, J. Wang, T. K. Sham, X. Sun, *Adv. Func. Mater.* **2017,** *27,* 1606662.

[8] S. Rosenberg, A. Hintennach, *J. Power Sources* **2015,** *274,* 1043.

[9] Y. Hu, X. Han, Q. Zhao, J. Du, F. Cheng, J. Chen, *J. Mater. Chem. A* **2015,** *3,* 3320.